An Implementation of the Particle Swarm Optimization Algorithm in Optimizing Fuzzy Logic Control for DC-Link Voltage Regulation in SAPF Systems

Zaenab Muslimin
Department of Electrical Engineering, Faculty of Engineering, Hasanuddin University, Indonesia
zaenab@unhas.ac.id (corresponding author)

Indar Chaerah Gunadin
Department of Electrical Engineering, Faculty of Engineering, Hasanuddin University, Indonesia
indar@eng.unhas.ac.id

Fitriyanti Mayasari
Department of Electrical Engineering, Faculty of Engineering, Hasanuddin University, Indonesia
fitriyanti maya@unhas.ac.id

Hendra Bara'langi'
Department of Electrical Engineering, Faculty of Engineering, Hasanuddin University, Indonesia
hendrabaralangi13@gmail.com

Received: 5 August 2025 | Revised: 28 September 2025 | Accepted: 5 October 2025

 DOI: https://doi.org/10.48084/etasr.13868

ABSTRACT

The increased use of electronic devices has caused power quality issues in the form of harmonic distortion. Shunt Active Power Filter (SAPF) offers a more effective and adaptable solution for reducing harmonics. This study aims to model, simulate, and evaluate the performance of the SAPF with DC-link voltage control using a Fuzzy Logic Controller (FLC) that is automatically optimized with the Particle Swarm Optimization (PSO) algorithm. The SAPF employs the instantaneous power theory approach to calculate the reference compensation current and a Hysteresis Current Controller (HCC) to operate the inverter and generate the appropriate compensation current. The simulation results show that without the SAPF, the current Total Harmonic Distortion (THD) reaches 20.77% and the voltage THD 4.83%. The basic implementation of the SAPF reduced the current THD to approximately 1.35% and the voltage THD to approximately 1.13%. The addition of FLC successfully decreased the current THD to around 0.71% and the voltage THD to about 0.55%, with a DC-link voltage overshoot of 1.06% and a Steady-State Error (SSE) of 0.41%. Applying FLC optimized with PSO significantly enhanced the performance, reducing the current THD to 0.36% and voltage THD to 0.35%, lowering the DC-link voltage overshoot to 0.85%, and decreasing the SSE to 0.31%. This study concludes that optimizing the FLC with PSO significantly improves the DC-link voltage control and the effectiveness of the SAPF in diminishing harmonics.

Keywords-shunt active power filter; fuzzy logic controller; particle swarm optimization; harmonic; dc-link control

I. INTRODUCTION

The advancement of semiconductor-based technologies has made harmonic distortion a critical concern in contemporary electric power systems. A wide variety of non-linear loads, including office equipment, air conditioners, Compact Fluorescent Lamps (CFLs), motor drives, and various household appliances, contribute significantly to THD, thereby affecting the power quality in distribution and transmission networks. Authors in [1] highlight that the proliferation of non-linear loads, such as personal computers and CFLs, in commercial buildings has adverse effects on power quality, as these loads inject harmonics into the network. Although the impact of each of these loads may appear minimal, their cumulative effect in a commercial center or residential area can impose substantial harmonic strain on the electric distribution system. In addition to the impact of the power system loads, the integration of renewable energy sources further complicates harmonic management, especially at the Point of Common Coupling (PCC). Harmonics in power systems lead to adverse effects such as equipment overheating, reduced device lifetime, and malfunctions in protection systems [2]. As stated in [3], Passive Power Filters (PPFs) and Active Power Filters (APFs) are the primary solutions widely used for harmonic mitigation. PPFs, which utilize passive elements, such as capacitors and inductors, are effective at absorbing specific harmonic frequencies under steady-state conditions. However, their limited adaptability and susceptibility to resonance render them less suitable for modern dynamic power systems. Conversely, APFs offer greater flexibility through control techniques that actively inject compensation currents to eliminate the harmonic components. This technology enables real-time adaptive harmonic control that can respond to the load fluctuations and varying grid conditions.

Among the various types of Active Power Filters, the SAPF is widely employed because of its simple configuration and mature technology [4]. The SAPF operates in parallel with the load, injecting a compensation current directly at the PCC to cancel out the harmonic components, reactive power, and current imbalances in real time [5]. The practical success of this technology is evident in [6], which describes the implementation of an SAPF, specifically for mitigating the severe harmonics from CFLs, achieving a remarkable reduction in THD from 89.6% to 1.62%. For an SAPF to function optimally, the stability of the DC-link voltage on the inverter side is crucial. This voltage supplies the necessary energy for the inverter to generate a compensation current with precise amplitude and phase. Without proper regulation, the fluctuations in the DC-link voltage caused by switching losses or load changes can degrade the accuracy of the compensation. For regulating the DC-link voltage, methods such as the Proportional-Integral (PI) controller and the FLC are commonly used [3].

PI or PID controllers are typically employed due to their simplicity in controlling the DC-link voltage. However, their design is based on linear system models, whereas the SAPF is an inherently non-linear system, whose behavior changes with load variations and network conditions. Consequently, conventional PI controllers often exhibit unsatisfactory performance during system transients. Authors in [7] demonstrated that an FLC-based DC-link voltage control is significantly more effective in reducing harmonics under balanced, unbalanced, and non-sinusoidal conditions compared to a PI controller. Similarly, in [8], it was shown that FLC delivers superior performance over a PI controller under dynamic loading conditions. Authors in [9] also highlighted this performance gap, showing a reduction in THD from 30.82% to 9.46% for PI, 8.47% for PID, and an impressive 4.74% for FLC. Despite their superior performance compared to conventional PI/PID controllers, FLCs remain challenging to design effectively. A PI controller requires the tuning of only two parameters (Kp and Ki), whereas a simple FLC with two inputs (such as error and error change) and seven triangular membership functions per input alone involves dozens of tunable parameters, including the position and width of each membership function. Furthermore, the rule base consists of 49 rules, each with its own output value to adjust. When scale factors are also included, the total number of parameters to be optimized can easily reach hundreds. This exponential expansion of the design space is a classic example of the curse of dimensionality. The difficulty of navigating this complex landscape has been recognized as a primary drawback of FLCs. Research has identified this issue, describing manual tuning as a time-consuming and tedious process and explicitly citing the curse of dimensionality as a factor that makes setting up a large rule base nearly impossible in practice [10].

To overcome these complex tuning challenges, intelligent optimization techniques based on metaheuristic algorithms are considered effective tools for automatically determining the optimal FLC parameters. Several studies have demonstrated the effectiveness of these methods, particularly those that employ PSO in tuning FLCs without the need for manual trial-and-error procedures [11-13]. However, in the specific domain of SAPF control, most research on intelligent tuning has focused on optimizing conventional PI controllers, as reported in [14, 15]. As a result, the application of metaheuristic-based tuning specifically for FLCs in SAPF systems remains relatively underexplored.

The present study applies PSO to automatically optimize the membership functions and the rule base of an FLC, aiming to address the research gap concerning FLC-PSO studies for SAPF applications. The objective function is formulated based on key system performance parameters, including overshoot, settling time, steady-state DC-link voltage error, and the overall harmonic reduction achieved by the SAPF.

II. METHODS

The system model consists of a three-phase network that includes an ideal sinusoidal voltage source, line impedance, and a nonlinear load in the form of an uncontrolled three-phase rectifier, as shown in Figure 1. The harmonic currents generated by the load cause voltage distortion at the PCC. To compensate for this, a Voltage Source Inverter (VSI)-based SAPF was designed and simulated. The detailed system parameters are summarized in Table I.

TABLE I. SYSTEM PARAMETERS

Supply voltage (VLL)	400 V
Frequency	50 Hz
DC-link capacitor	1000 uF
Coupling inductor	1 mH
Linear load	5 kW ‖ 10 kVAR
Non-linear load	28 kW (3-phase diode rectifier)

The nonlinear load is modeled as a three-phase diode bridge rectifier supplying an R–L load on the DC side. This configuration is widely used to emulate industrial nonlinear loads such as adjustable-speed drives and power converters. At the AC side, the rectifier draws a highly distorted current waveform with a total demand of 28 kW, producing significant low-order harmonics, mainly the 5th, 7th, 11th, and 13th orders.

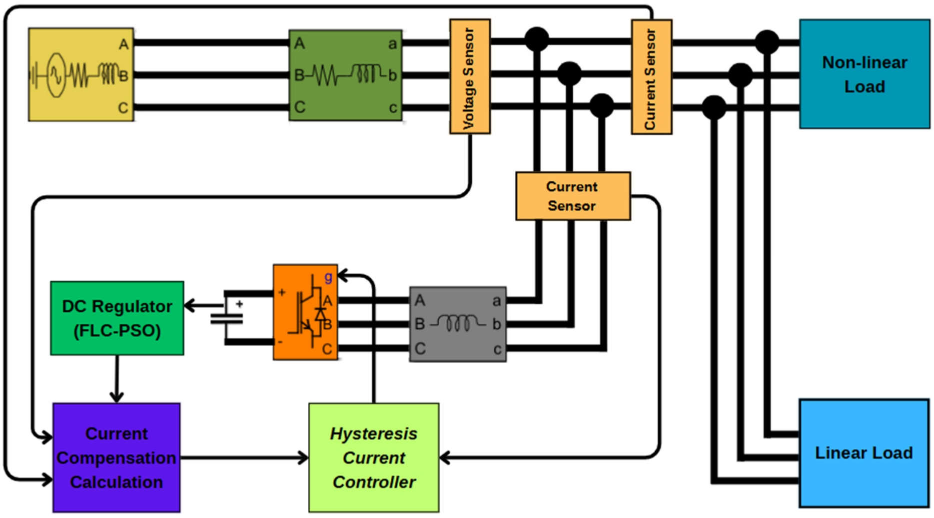

Fig. 1. SAPF block diagram.

The SAPF is based on a three-phase VSI topology using power transistors. A DC-link capacitor provides the necessary energy storage to generate the compensation current, and the DC-link regulator/controller maintains a stable DC voltage. The VSI is connected to the PCC through a coupling inductor of 1 mH, which serves to smooth the high-frequency switching ripples from the injected compensation current. The instantaneous power theory (p–q theory) [16] is employed for the generation of the reference compensation current. This method is one of the most widely adopted techniques for SAPF control [17]. This theory provides a mathematical approach for analyzing and controlling power in a three-phase system through the Clarke transformation that converts the three-phase voltage and current variables (v_a, v_b, v_c, i_a, i_b, and i_c) into a two-dimensional orthogonal coordinate system (α, β), thereby facilitating the separation of instantaneous active and reactive power components [18, 19]. The Clarke transformation is expressed by:

$$\begin{bmatrix} v_0 \\ v_\alpha \\ v_\beta \end{bmatrix} = \sqrt{\frac{2}{3}} \begin{bmatrix} \frac{1}{\sqrt{2}} & \frac{1}{\sqrt{2}} & \frac{1}{\sqrt{2}} \\ 1 & \frac{-1}{2} & \frac{-1}{2} \\ 0 & \frac{\sqrt{3}}{2} & \frac{-\sqrt{3}}{2} \end{bmatrix} \begin{bmatrix} v_a \\ v_b \\ v_c \end{bmatrix} \quad (1)$$

$$\begin{bmatrix} i_0 \\ i_\alpha \\ i_\beta \end{bmatrix} = \sqrt{\frac{2}{3}} \begin{bmatrix} \frac{1}{\sqrt{2}} & \frac{1}{\sqrt{2}} & \frac{1}{\sqrt{2}} \\ 1 & \frac{-1}{2} & \frac{-1}{2} \\ 0 & \frac{\sqrt{3}}{2} & \frac{-\sqrt{3}}{2} \end{bmatrix} \begin{bmatrix} i_a \\ i_b \\ i_c \end{bmatrix} \quad (2)$$

The voltage and current that have been transformed to the α–β domain are used to calculate the active power (p) and reactive power (q), as shown in:

$$\begin{bmatrix} p_0 \\ p \\ q \end{bmatrix} = \begin{bmatrix} v_0 & 0 & 0 \\ 0 & v_\alpha & v_\beta \\ 0 & v_\beta & -v_\alpha \end{bmatrix} \begin{bmatrix} i_0 \\ i_\alpha \\ i_\beta \end{bmatrix} \quad (3)$$

The calculated power values consist of both DC ($\bar{p}$, $\bar{q}$) and AC ($\tilde{p}$, $\tilde{q}$) components, as shown in (4). The AC components correspond to the harmonic distortion and are extracted using a digital Low-Pass Filter (LPF) to be targeted for compensation:

$$\begin{aligned} p &= \bar{p} + \tilde{p} \\ q &= \bar{q} + \tilde{q} \end{aligned} \quad (4)$$

To maintain DC-link voltage stability, the controller is based on a zero-order Takagi-Sugeno fuzzy inference system, chosen for its computational efficiency and suitability for optimization applications compared to Mamdani-type systems [20]. The overall structure of the proposed fuzzy logic controller, implemented in MATLAB/Simulink, is illustrated in Figure 2.

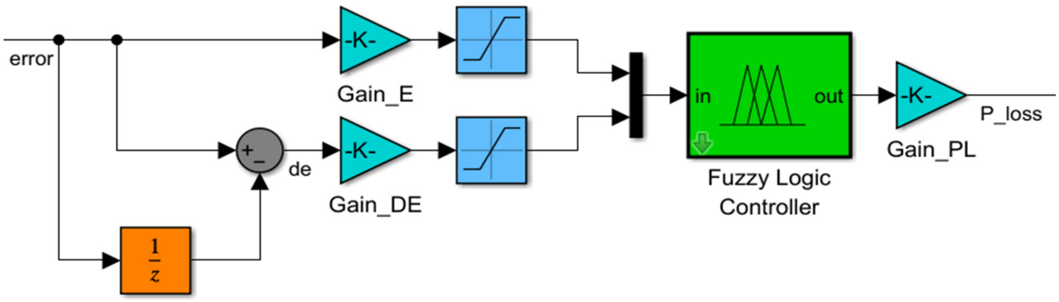

Fig. 2. Fuzzy logic controller.

The FLC is designed with two input variables: error (e), defined as the difference between the actual DC-link voltage and its reference, and Δerror (Δe), defined as the rate of change of error. Both input variables were normalized within the range [-1,1] and represented by five Gaussian membership functions: Negative Big (NB), Negative Small (NS), Zero (ZE), Positive Small (PS), and Positive Big (PB), as depicted in Figure 3.

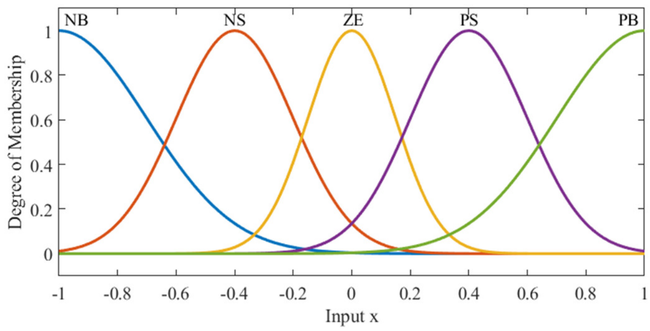

Fig. 3. Input membership function.

The Gaussian membership function is mathematically expressed as [21]:

$$\mu(x) = \exp\left[-\frac{1}{2}\left(\frac{x_i - c_i}{\sigma_i}\right)^2\right] \quad (5)$$

where c_i and σ_i represent the center and width of the i-th Gaussian function, respectively.

The output variable, p_loss, which corresponds to the required active power compensation, is represented by seven singleton membership functions: NB, Negative Medium (NM), NS, ZE, PS, Positive Medium (PM), and PB. These are uniformly distributed within the range [−1,1], as presented in Table II.

TABLE II. OUTPUT VARIABLE

NB	NM	NS	ZE	PS	PM	PB
-1	-0.6	-0.25	0	0.25	0.6	1

The rule base is constructed using the classical approach of mapping error and Δerror into the corresponding control action. The 5×5 rule matrix is portrayed in Table III, which defines the fuzzy relationship between the two inputs and the output.

TABLE III. RULE BASE

error \ Δerror	NB	NS	ZE	PS	PB
NB	NB	NB	NM	NS	ZE
NS	NM	NS	NS	ZE	PS
ZE	NM	NS	ZE	PS	PM
PS	NS	ZE	PS	PS	PM
PB	ZE	PS	PM	PB	PB

The defuzzification process uses the weighted average method to produce a crisp output (p_loss), which represents the required active power compensation. For defuzzification, the weighted average method is employed [21]:

$$z^* = \frac{\sum \mu_{\underset{\sim}{C}}(\bar{z}) \cdot \bar{z}}{\sum \mu_{\underset{\sim}{C}}(\bar{z})} \quad (6)$$

where $\mu_{\underset{\sim}{C}}(\bar{z})$ is the degree of membership of the output fuzzy set, and $\bar{z}$ is the corresponding singleton value.

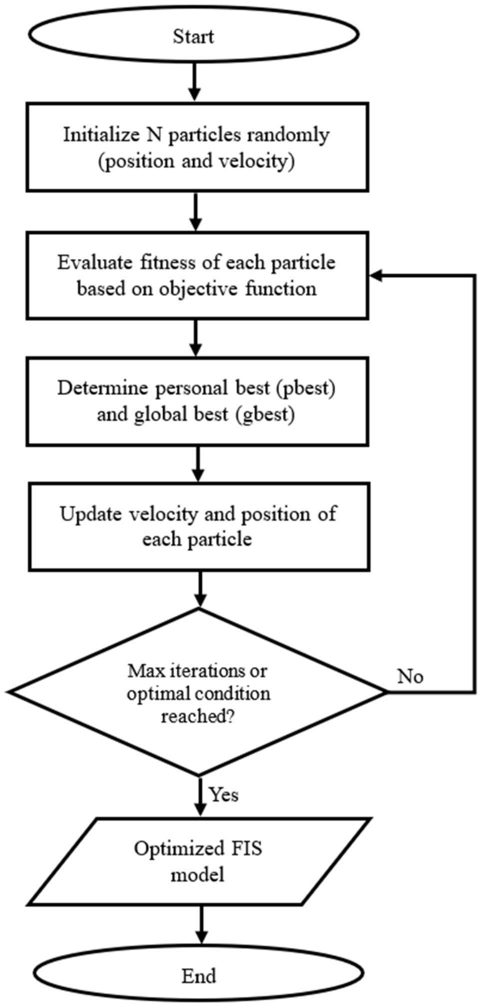

Fig. 4. PSO flowchart.

To overcome the challenges of manual tuning and the "curse of dimensionality" inherent in FLC design, the PSO algorithm was employed. The PSO, a population-based stochastic optimization technique [22], is well-suited for navigating complex, high-dimensional search spaces. The algorithm iteratively adjusts the population of candidate solutions (particles) to determine the optimal set of FLC parameters. The operational steps of the PSO algorithm applied in this work are summarized in Figure 4. The objective function for the PSO was formulated to minimize the weighted sum of five key performance metrics, as shown in:

$$J = w_1 \cdot OS + w_2 \cdot ST + w_2 \cdot SSE + w_3 \cdot ITAE + w_4 \cdot THD \quad (7)$$

where OS is the overshoot, ST is the Settling Time, SSE is the Steady-State Error, ITAE is the Integral of the Time-weighted Absolute Error of the DC-link voltage response, and THD is the Total Harmonic Distortion of the source current.

The reference current is calculated using (8) based on the selected harmonic and reactive power components:

$$\begin{bmatrix} i_\alpha^* \\ i_\beta^* \end{bmatrix} = \frac{1}{v_\alpha^2+v_\beta^2}\begin{bmatrix} v_\alpha & v_\beta \\ v_\beta & -v_\alpha \end{bmatrix}\begin{bmatrix} -p_c^* + p_{loss} \\ -q_c^* \end{bmatrix} \quad (8)$$

Next, the inverse transformation from the *α–β* domain to the three-phase coordinate system (*a–b–c*) is shown by:

$$\begin{bmatrix} i_a \\ i_b \\ i_c \end{bmatrix} = \sqrt{\frac{2}{3}}\begin{bmatrix} \frac{1}{\sqrt{2}} & 1 & 0 \\ \frac{1}{\sqrt{2}} & \frac{-1}{2} & \frac{\sqrt{3}}{2} \\ \frac{1}{\sqrt{2}} & \frac{-1}{2} & \frac{-\sqrt{3}}{2} \end{bmatrix}\begin{bmatrix} i_0 \\ i_\alpha \\ i_\beta \end{bmatrix} \quad (9)$$

Once the final reference currents are generated, a current control technique is required to produce the corresponding gate signals for the VSI. For this purpose, an HCC was employed. This method, a form of control without an external modulator, was selected for its well-known advantages, including simple implementation, high accuracy, and a very fast dynamic response [23, 24]. HCC operates by comparing the measured SAPF current with the generated reference current and confining the resulting error within a predefined hysteresis band. If the error exceeds the upper or lower boundary, the controller instantly sends an appropriate switching command to the VSI gates to force the error back within the band.

System performance evaluation was conducted through four simulation scenarios. The first scenario was the baseline condition without SAPF to observe the initial harmonic characteristics. In the second scenario, the SAPF was activated using the *p–q* method without DC-link voltage control. The third scenario adds an FLC, whereas the fourth scenario uses an FLC optimized with PSO. All scenarios were run under identical system and load conditions.

The data collected from the simulations included the voltage and current on the source and load sides, reference and actual currents from the SAPF, and DC-link voltage response. An analysis was conducted on the controller performance parameters and harmonic compensation effectiveness. The THD value was analyzed using Fast Fourier Transform (FFT), whereas the DC-link voltage stability indicator was evaluated based on the transient response and steady-state error.

III. RESULTS AND DISCUSSION

The effectiveness of the SAPF configuration was evaluated based on four simulation scenarios. Table IV summarizes the main results, including the source current THD, power factor, and DC-link voltage stability.

Under uncompensated conditions (Scenario 1), the system exhibited a high current distortion (THDi ≈ 20.77%) owing to nonlinear loads dominated by an uncontrolled three-phase bridge rectifier. As expected, this condition also caused voltage distortion (THDv ≈ 4.83%) at the PCC due to line impedance in the power system.

The implementation of the SAPF based on the *p–q* theory (Scenario 2) successfully reduced the current distortion to around 1.35%, voltage distortion to around 1.13%, and increased the power factor from 0.90 to 0.99. These results demonstrate that the SAPF is highly effective in injecting reactive and harmonic compensation currents to improve power quality.

TABLE IV. SUMMARY OF SIMULATION RESULTS

Parameters	**Scenarios**			
	Without SAPF	**SAPF without voltage control**	**SAPF with FLC**	**SAPF with FLC-PSO**
THDv R	4.83%	1.12%	0.54%	0.35%
THDv S	4.83%	1.10%	0.54%	0.35%
THDv T	4.83%	1.16%	0.58%	0.34%
THDi R	20.77%	1.34%	0.70%	0.36%
THDi S	20.77%	1.32%	0.68%	0.37%
THDi T	20.77%	1.40%	0.74%	0.36%
Power factor	0.90	0.99	0.99	0.99
Overshoot	-	-	1.06%	0.85%
Settling time	-	-	0.062s	0.065s
Steady-state error	-	-	0.41%	0.31%

As explained in [16], SAPF is designed based on the *p–q* theory and functions as a compensator, which ideally does not involve net energy exchange between the filter and the electrical network. However, in practice, there are unavoidable internal power losses in the physical components of the filter. If harmonic compensation occurs ideally, the energy stored in the DC-link capacitor will continue to be used to cover these losses, ultimately dissipated as heat [25]. As a result, the voltage across the DC-link capacitor will gradually decrease, affecting the SAPF's ability to inject reference compensation current. Therefore, SAPF without DC-link voltage control cannot guarantee long-term operational stability. As shown in Figure 5, without voltage control, the DC-link capacitor experiences a continuous increase in voltage. This condition indicates that the SAPF designed based on the *p–q* theory cannot provide perfect harmonic compensation. This imperfect compensation can be explained by Figure 6, which shows a difference between the reference current and the actual current, where the actual current has a larger magnitude. This overcompensation behavior is caused by using low-pass or high-pass filters to calculate the reference current based on the *p–q* theory, which introduces a signal delay. Additionally, current control using the HCC method contributes to response inaccuracy because it operates within the hysteresis band.

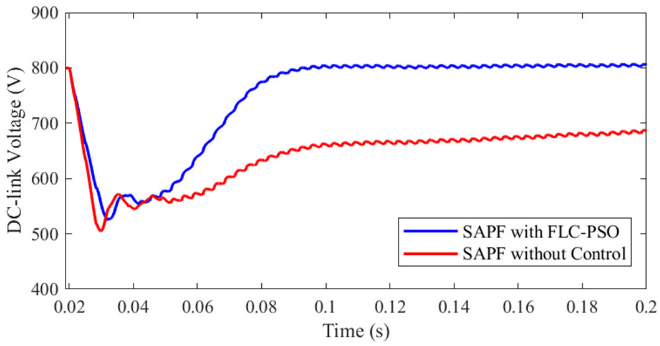

Fig. 5. Comparison of the DC-link voltage.

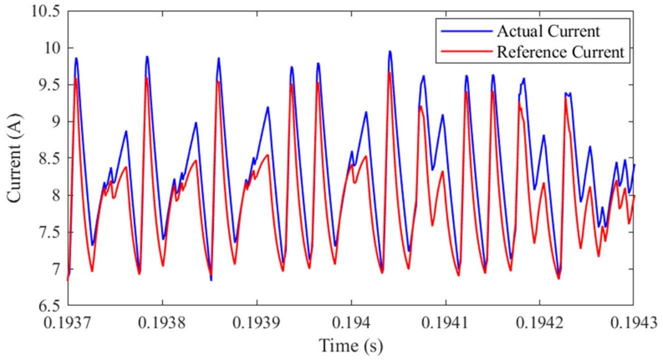

Fig. 6. Comparison of the reference current and actual current from VSI SAPF.

The application of Fuzzy Logic Control in Scenario 3 to actively regulate the DC-link voltage around a reference value of 800 V resulted in improved system stability. The simulation results show a reduction in the overshoot to 1.06%, an SSE of 0.41%, and an ITAE value of 0.49 Vs. This improvement also contributed to enhanced SAPF performance, as evidenced by the reduction in THDi to an average of ~0.71% and THDv to ~0.55%. FLC compensates for active power losses (p_loss) through fuzzy mapping between error signals and their derivatives. This approach produces an adaptive response to load changes, making SAPF more reliable in dealing with system dynamics [6].

Scenario 4 applies the PSO algorithm to automatically adjust the FLC parameters to optimize the controller design. This approach addresses the complexity and inefficiency of manual adjustments in fuzzy systems with a vast parameter space. PSO adaptively seeks the optimal combination of FLC parameters to enhance the DC-link voltage stability and harmonic reduction effectiveness.

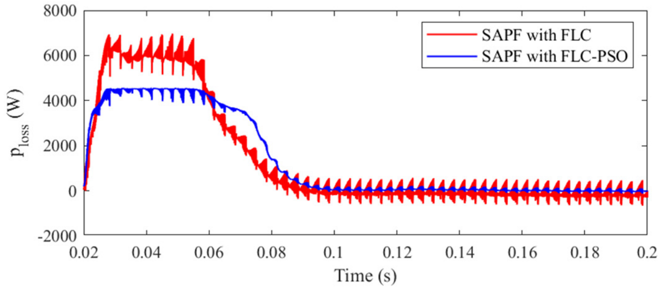

Fig. 7. Comparison of additional power estimates by fuzzy logic control.

The FLC-PSO-based controller demonstrated superior performance, with a lower overshoot (0.85%) and an SSE of 0.31%, despite a slight increase in settling time. This trade-off is reasonable in multi-criteria optimization because the PSO algorithm inherently strives to balance conflicting performance metrics. The THDi value decreases to approximately 0.36%, and the THDv becomes approximately 0.35%, the lowest among all scenarios. According to the IEEE standards, these current and voltage harmonic values are below the maximum permissible thresholds. Figure 7 shows that FLC-PSO control can estimate additional power requirements more accurately and efficiently, while reducing the tendency for overcompensation that previously caused a continuous increase in DC-link voltage. Additionally, during transient conditions, the FLC helps the system reach a steady state more quickly.

The load used in this study was an uncontrolled three-phase bridge rectifier, which produced harmonic components of order 6k±1, where k is a positive integer. The comparison of the changes in Individual Harmonic Distortion (IHD) in each phase is displayed in Figure 8.

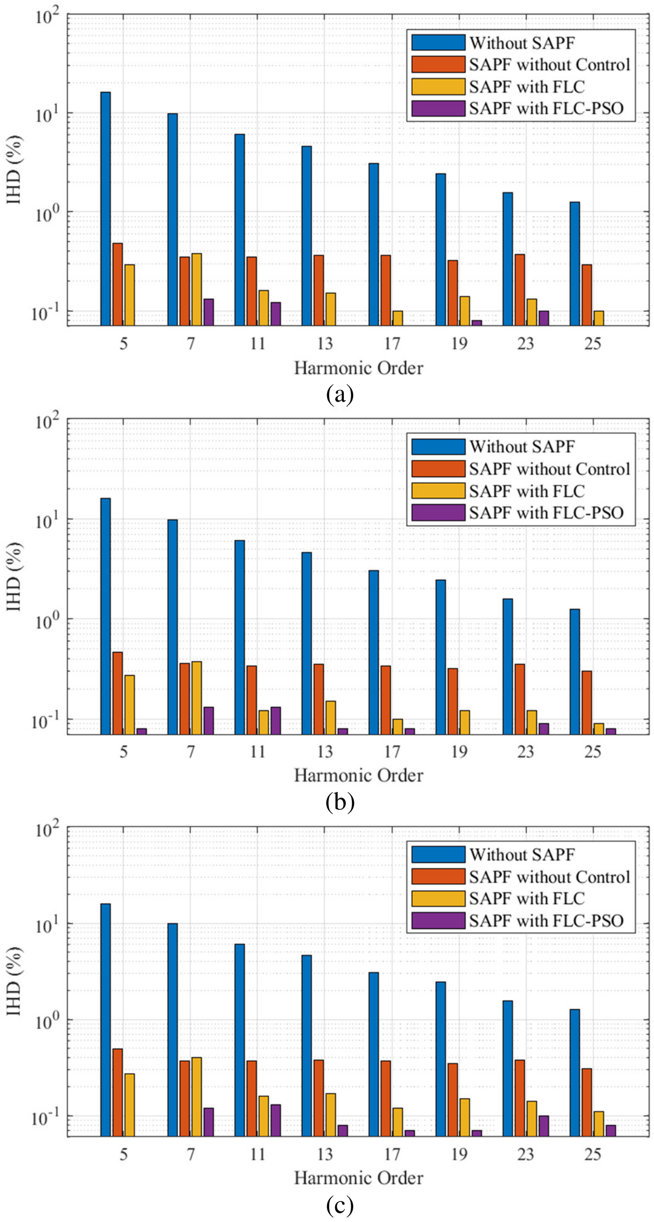

Fig. 8. (a) Comparison of dominant IHD in phase R, (b) comparison of dominant IHD in phase S, (c) comparison of dominant IHD in phase T.

The change in the current waveform from a distorted condition to one close to sinusoidal can be observed in Figure 9, which compares the three-phase current before and after compensation. After applying the FLC-PSO-based SAPF, the current waveform approaches a pure sinusoidal shape, indicating an overall improvement in power quality.

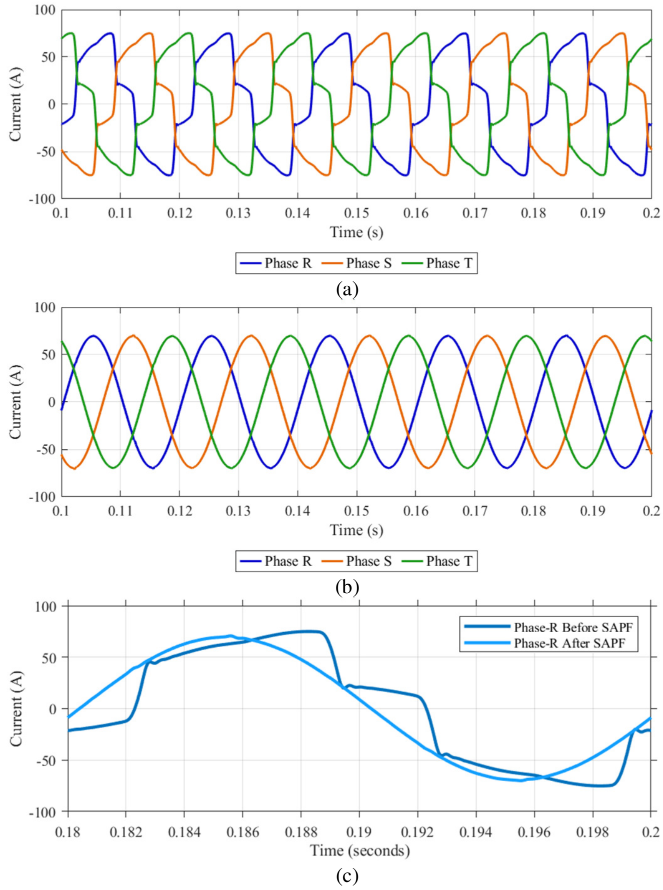

Fig. 9. (a) 3-phase current without SAPF, (b) 3-phase current after installing SAPF FLC-PSO, (c) zoomed-in comparison for Phase-R over one cycle.

IV. CONCLUSIONS

This study used an optimization method that combined a Fuzzy Logic Controller (FLC) with a Particle Swarm Optimization (PSO) algorithm to improve the performance of the Shunt Active Power Filter (SAPF) in harmonic reduction. This method demonstrates superior performance in suppressing harmonic distortion, as evidenced by its success in reducing the current's Total Harmonic Distortion (THD) from 20% to below 1%, meeting IEEE power quality standards. Applying FLC-PSO in DC-link voltage control can control the voltage at the reference value with an overshoot of 0.85%, a settling time of 0.065 s, and an SSE of 0.31%.

Future research directions will focus on validating this method by implementing hardware-in-the-loop or physical prototypes to test its robustness under real-world operational conditions. Additionally, comparisons with other intelligent methods could provide new insights into achieving a more optimal balance between computational speed and accuracy.

ACKNOWLEDGEMENT

The authors would like to thank the Faculty of Engineering, Hasanuddin University, for supporting the Laboratory-Based Education (LBE) Excellence Innovation Research Scheme under contract number xxxx/UN4.7.2/PM.01.01/2025.

REFERENCES

[1] T. Mathwai, K. Awodele, and A. Ojo, "Power Quality Evaluation of Electrical Loads in a Typical Commercial Building," in *2020 International SAUPEC/RobMech/PRASA Conference*, Cape Town, South Africa, Jan. 2020, pp. 1–6, https://doi.org/10.1109/SAUPEC/RobMech/PRASA48453.2020.9041007.

[2] R. R. Stanley, "Chapter 7 - Power quality improvements for renewable power plants," in *Power Systems Operation with 100% Renewable Energy Sources*, S. Chenniappan, S. Padmanaban, and S. Palanisamy, Eds. Elsevier, 2024, pp. 85–107.

[3] Z. M. Ali, M. Ćalasan, F. Jurado, and S. H. E. Abdel Aleem, "Complexities of Power Quality and Harmonic-Induced Overheating in Modern Power Grids Studies: Challenges and Solutions," *IEEE Access*, vol. 12, pp. 151554–151597, 2024, https://doi.org/10.1109/ACCESS.2024.3477729.

[4] D. Li, T. Wang, W. Pan, X. Ding, and J. Gong, "A comprehensive review of improving power quality using active power filters," *Electric Power Systems Research*, vol. 199, Oct. 2021, Art. no. 107389, https://doi.org/10.1016/j.epsr.2021.107389.

[5] M. Popescu, A. Bitoleanu, C. V. Suru, M. Linca, and L. Alboteanu, "Shunt Active Power Filters in Three-Phase, Three-Wire Systems: A Topical Review," *Energies*, vol. 17, no. 12, Jan. 2024, Art. no. 2867, https://doi.org/10.3390/en17122867.

[6] M. Hajjej and L. Sbita, "A New Design and Implementation of a Three-Phase Four-Wire Shunt Active Power Filter for Mitigating Harmonic Problems caused by Compact Fluorescent Lamps," *Engineering, Technology & Applied Science Research*, vol. 14, no. 3, pp. 14619–14627, Jun. 2024, https://doi.org/10.48084/etasr.7251.

[7] S. Mikkili and A. K. Panda, "SHAF for Mitigation of Current Harmonics Using p-q Method with PI and Fuzzy Controllers," *Engineering, Technology & Applied Science Research*, vol. 1, no. 4, pp. 98–104, Aug. 2011, https://doi.org/10.48084/etasr.44.

[8] P. K. Barik, G. Shankar, and P. K. Sahoo, "DC-Link Capacitor Voltage Stabilization of a Shunt Active Power Filter Using Fuzzy Logic Controller Under Dynamic Loading Condition," in *Proceedings of Symposium on Power Electronic and Renewable Energy Systems Control*, Singapore, 2021, pp. 403–414, https://doi.org/10.1007/978-981-16-1978-6_35.

[9] K. Hemasri and C. S. Kumar, "Fuzzy Controller with Shunt Active Power Filter in Reducing THD for Three Phase System," *International Transactions on Electrical Engineering and Computer Science*, vol. 3, no. 2, pp. 101–108, Jun. 2024, https://doi.org/10.62760/iteecs.3.2.2024.93.

[10] S. M. Belhadj, B. Meliani, H. Benbouhenni, S. Zaidi, Z. M. S. Elbarbary, and M. M. Alammar, "Control of multi-level quadratic DC-DC boost converter for photovoltaic systems using type-2 fuzzy logic technique-based MPPT approaches," *Heliyon*, vol. 11, no. 3, Feb. 2025, Art. no. e42181, https://doi.org/10.1016/j.heliyon.2025.e42181.

[11] J. L. da Silva, "Fuzzy Logic Control with PSO Tuning," in *Fuzzy Systems - Theory and Applications*, IntechOpen, 2021.

[12] K. R. Bharath Kumar, P. Senthil Kumar, K. S. Dharaneeshwarakumar, and B. Deepak, "Particle Swarm Optimization Tuned Fuzzy Controller for Vibration Control of Active Suspension System," in *Advances in Materials Research*, Singapore, 2021, pp. 115–125, https://doi.org/10.1007/978-981-15-8319-3_13.

[13] M. A. R. Shafei, D. K. Ibrahim, and M. Bahaa, "Application of PSO tuned fuzzy logic controller for LFC of two-area power system with redox flow battery and PV solar park," *Ain Shams Engineering Journal*, vol. 13, no. 5, Sep. 2022, Art. no. 101710, https://doi.org/10.1016/j.asej.2022.101710.

[14] A. M. Hadi, E. M. Thajeel, and A. K. Nahar, "A novel optimizing PI control of shunt active power filter for power quality enhancement," *Bulletin of Electrical Engineering and Informatics*, vol. 11, no. 3, pp. 1194–1202, Jun. 2022, https://doi.org/10.11591/eei.v11i3.3225.

[15] S. A. A. Shukor, W. A. Halim, A. Razi, M. A. Mohd Radzi Advanced, N. F. Mailah, and M. L. Othman, "An Optimal Tuning of PI Controller for Shunt Active Power Filter Based on PI-PSO Approach," in *2024 IEEE International Conference on Power and Energy (PECon)*, Kuala Lumpur, Malaysia, Nov. 2024, pp. 199–204, https://doi.org/10.1109/PECon62060.2024.10826925.

[16] S. K. Dash, P. K. Ray, and P. Ray, "Implementation of adaptive control strategies for PV system integrated unified conditioner for optimal power quality regulation," *Results in Engineering*, vol. 26, Jun. 2025, Art. no. 105122, https://doi.org/10.1016/j.rineng.2025.105122.

[17] A. M. Hadi, E. M. Thjeel, and A. K. Nahar, "A Review of Control Technique Applied in Shunt Active Power Filter (SAPF)," *Engineering and Technology Journal*, vol. 40, no. 8, pp. 1035–1044, Aug. 2022, https://doi.org/10.30684/etj.v40i8.2116.

[18] K. Naftahi, A. Abouloifa, Z. Hekss, S. Echalih, F. Ait bellah, and I. Lachkar, "Three-Phase Four-Wire Shunt Active Power Filter Based on the Hybrid Automaton Control with Instantaneous Reactive Power Theory," *IFAC-PapersOnLine*, vol. 55, no. 12, pp. 532–537, Jan. 2022, https://doi.org/10.1016/j.ifacol.2022.07.366.

[19] J. Mikulović and T. Šekara, "Power definitions for electrical circuits with nonsinusoidal and unbalanced voltages and currents," in *Encyclopedia of Electrical and Electronic Power Engineering*, J. García, Ed. Oxford: Elsevier, 2023, pp. 113–131.

[20] A. Atif, K. A. Khan, and M. Khalid, "17 - Solar power smoothing using battery energy storage system through fuzzy filtration technique," in *Emerging Trends in Energy Storage Systems and Industrial Applications*, Prabhansu and N. Kumar, Eds. Academic Press, 2023, pp. 485–520.

[21] G. Tayfur, "Chapter 10 - Application of fuzzy logic in water resources engineering," in *Handbook of Hydroinformatics*, S. Eslamian and F. Eslamian, Eds. Elsevier, 2023, pp. 155–166.

[22] D. Chauhan, Shivani, and P. N. Suganthan, "Learning strategies for particle swarm optimizer: A critical review and performance analysis," *Swarm and Evolutionary Computation*, vol. 98, Oct. 2025, Art. no. 102048, https://doi.org/10.1016/j.swevo.2025.102048.

[23] S. Mandal, *Sensors, Circuits, and Systems for Scientific Instruments*. Academic Press, 2026.

[24] M. D. Faraby, O. Penangsang, R. S. Wibowo, S. Sofyan, A. R. Idris, and A. Asri, "Harmonic Mitigation Through Enhancement Network Reconfiguration Technique on Coordinated Planning Using Hybrid Particle Swarm Optimization in Radial Distribution System," in *2021 3rd International Conference on Electrical, Control and Instrumentation Engineering*, Nov. 2021, pp. 1–6, https://doi.org/10.1109/ICECIE52348.2021.9664728.

[25] D. Çelik, "Lyapunov based harmonic compensation and charging with three phase shunt active power filter in electrical vehicle applications," *International Journal of Electrical Power & Energy Systems*, vol. 136, Mar. 2022, Art. no. 107564, https://doi.org/10.1016/j.ijepes.2021.107564.